Chapter 3
Classical Cyclotron

Abstract This chapter introduces the classical cyclotron, and the theoretical material needed for the simulation exercises. It begins with a brief reminder of the historical context, and continues with beam optics and with the principles and methods which the classical cyclotron leans on, including
- ion orbit in a cyclic accelerator,
- weak focusing and periodic transverse motion,
- revolution period and isochronism,
- voltage gap and resonant acceleration,
- the cyclotron equation.
The simulation of a cyclotron dipole will either resort to an analytical model of the field: the optical element DIPOLE, or will resort to using a field map together with the keyword TOSCA to handle it and raytrace through. An additional accelerator device needed in the exercises, CAVITE, simulates a local oscillating voltage. Running a simulation generates a variety of output files, including the execution listing zgoubi.res, always, and other zgoubi.plt, zgoubi.CAVITE.out, zgoubi.MATRIX.out, etc., aimed at looking up program execution, storing data for post-treatment, producing graphs, etc. Additional keywords are introduced as needed, such as the matching procedure FIT[2]; FAISCEAU and FAISTORE which log local particle data in zgoubi.res or in a user defined ancillary file; MARKER; the 'system call' command SYSTEM; REBELOTE, a 'do loop'; and some more. This chapter introduces in addition to spin motion in accelerator magnets; dedicated simulation exercises include a variety of keywords: SPNTRK, a request for spin tracking, SPNPRT or FAISTORE, to log spin vector components in respectively zgoubi.res or some ancillary file, and the "IL=2" flag to log stepwise particle data, including spin vector, in zgoubi.plt file. Simulations include deriving transport matrices, beam matrix, optical functions and their transport, from rays, using MATRIX and TWISS keywords.

1538 **Notations used in the Text**

B; B_0	magnetic field; at a reference radius R_0
$\mathbf{B}$; B_R; B_y	field vector; radial component; axial component
$BR = p/q$	magnetic rigidity
C; C_0	orbit length, $C = 2\pi R$; reference, $C_0 = 2\pi R_0$
E	ion energy, $E = \gamma m_0 c^2$
f_{rev}, f_{rf}	revolution and RF voltage frequencies
G	gyromagnetic anomaly, $G = 1.7928$ for proton, -4.184 for helion
h	harmonic number, an integer, $h = f_{\text{rf}}/f_{\text{rev}}$
$k = \frac{R}{B}\frac{dB}{dR}$	radial field index
m; m_0; M	ion mass; rest mass; in units of MeV/c^2
$\mathbf{p}$; p; p_0	ion momentum vector; its modulus; reference
q	ion charge
R; R_0; R_E	equilibrium orbit radius; reference, $R(p_0)$; at energy E
RF	Radio-Frequency
1539 s	path variable
T_{rev}, T_{rf}	revolution and accelerating voltage periods
$\mathbf{v}$; v	ion velocity vector; its modulus
$V(t)$; $\hat{V}$	oscillating voltage; its peak value
W	kinetic energy, $W = \frac{1}{2}mv^2$
x, x', y, y'	radial and axial coordinates $\left[(*)' = \frac{d(*)}{ds}\right]$
α	trajectory deviation, or momentum compaction
$\beta = \frac{v}{c}$; β_0; β_s	normalized ion velocity; reference; synchronous
$\gamma = E/m_0 c^2$	Lorentz relativistic factor
Δp, δp	momentum offset
ε_u	Courant-Snyder invariant (u : x, r, y, l, Y, Z, s, etc.)
θ	azimuthal angle
ϕ	RF phase at ion arrival at the voltage gap

1540 **3.1 Introduction**

1541 Cyclotrons are the most widespread type of accelerator, today, used by thousands,
1542 with the production of isotopes as the dominant application. This chapter is devoted
1543 to the first cyclic accelerator: the early 1930s *classical* cyclotron which its concept
1544 limited to low energy, a few 10s of MeV/nucleon. This limitation overcome a decade
1545 later by the azimuthally varying field (AVF) technique, this is the subject of the next
1546 chapter.

1547   The classical cyclotron is based on four main principles:
1548 (i) the use of a cylindrical-symmetry magnetic field in the gap of an electromagnet
1549 (Fig. 3.1) to maintain ions on a circular trajectory

¹⁵⁵⁰ (ii) transverse vertical confinement of the beam obtained by a slow radial decrease
¹⁵⁵¹ of the magnetic field. A technique known as weak focusing, applied over the years
¹⁵⁵² in all cyclic accelerators: microtron, betatron, synchrocyclotron, synchrotron. These
¹⁵⁵³ weak focusing accelerator species all are still part of the landscape today
¹⁵⁵⁴ (iii) resonant acceleration by synchronization of a fixed-frequency accelerating volt-
¹⁵⁵⁵ age on the quasi-constant revolution time (Fig. 3.1). and
¹⁵⁵⁶ (iv) use of high voltage, to mitigate the effect of the turn-by-turn RF phase slip.

¹⁵⁵⁷ Resonant acceleration has the advantage that a small gap voltage is enough to
¹⁵⁵⁸ accelerate with, in principle, no energy limitation, by contrast with the electrostatic
¹⁵⁵⁹ techniques developed at the time, which required the generation of the full voltage,
¹⁵⁶⁰ such as the Van de Graaf which was limited by sparking at a few tens of megavolts.

¹⁵⁶¹ The cyclotron concept goes back to the late 1920s [1], yet it was not until the early
¹⁵⁶² 1930s when a cyclotron was first brought to operation [2]. The principles are sum-
¹⁵⁶³ marized in Fig. 3.1: an oscillating voltage is applied on a pair of electrodes ("dees")
¹⁵⁶⁴ forming an accelerating gap and placed between the two poles of an electromagnet.
¹⁵⁶⁵ Ions reaching the gap during the acceleration phase of the voltage wave experience
¹⁵⁶⁶ an energy boost; no field is experienced inside the dees. Under the effect of energy
¹⁵⁶⁷ increase at the gap every half-revolution, they spiral out in the quasi-constant field
of the dipole.
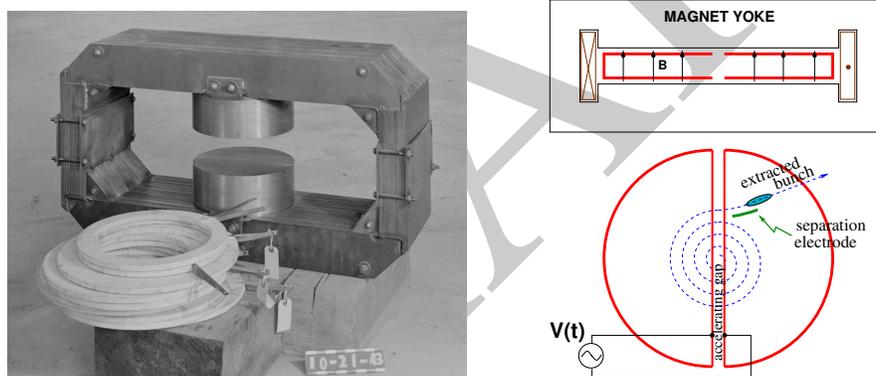
Fig. 3.1 Left: a cyclotron electromagnet, namely here that used for a model of Berkeley's 184-inch cyclotron in the early 1940s [3]. Magnetic field in the gap decreases with radius. Right: a schematic of the resonant acceleration motion; gap after gap, accelerated ions spiral out (bottom) in the quasi-uniform field (top). A double-dee (or, a variant, a single-dee facing a slotted electrode) forms an accelerating gap. The fixed-frequency oscillating voltage $V(t)$ applied is a harmonic of the revolution frequency. Ions experiencing proper voltage phase at the gap, turn by turn, are accelerated. A septum electrode allows beam extraction

¹⁵⁶⁸
¹⁵⁶⁹ The first cyclotron achieved acceleration of H_2^+ hydrogen ions to $80\,keV$ [2], at
¹⁵⁷⁰ Berkeley in 1931. The apparatus used a dee-shaped electrode vis-à-vis a slotted
¹⁵⁷¹ electrode forming a voltage gap, the ensemble housed in a $5\,in$ diameter vacuum
¹⁵⁷² chamber and placed in the 1.3 Tesla field of an electromagnet. A $\approx 12\,MHz$ vacuum
¹⁵⁷³ tube oscillator provided $1\,kVolt$ gap voltage.

One goal foreseen in developing this technology was the acceleration of protons to MeV energy range for the study of atom nucleus. And in background, a wealth of potential applications. An 11 in cyclotron followed which delivered a 0.01 μA H_2^+ beam at 1.22 MeV [4], and a 27 in cyclotron later reached 6 MeV (Fig. 3.2) [5]. Targets were mounted at the periphery of the 11-inch cyclotron, disintegrations were observed in 1932. And, in 1933: *'The neutron had been identified by Chadwick in* 1932. *By* 1933 *we were producing and observing neutrons from every target bombarded by deuterons."* [5, M.S. Livingston, p. 22].
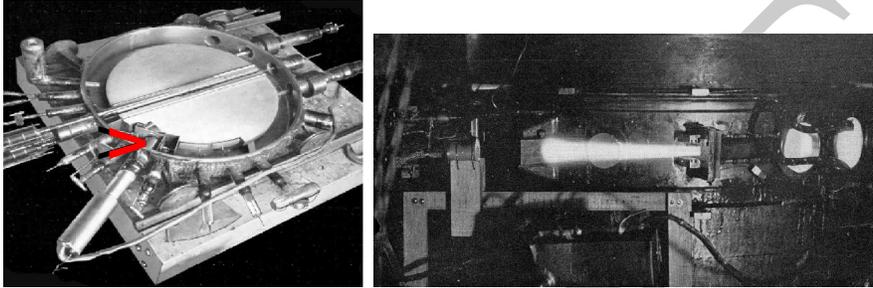

Fig. 3.2 Berkeley 27-inch cyclotron, brought to operation in 1934, accelerated deuterons up to 6 MeV. Left: a double-dee (seen in the vacuum chamber, cover off), 22 in diameter, creates an accelerating gap: 13 kV, 12 MHz radio frequency voltage is applied for deuterons for instance (through two feed lines seen at the top right corner). This apparatus was dipped in the 1.6 Tesla dipole field of a 27 in diameter, 75 ton, electromagnet. A slight decrease of the dipole field with radius, from the center of the dipole, ensures axial beam focusing. With their energy increasing, ions spiral out from the center to eventually strike a target (red arrow). Right: ionization of the air by the extracted beam (1936); the view also shows the vacuum chamber squeezed between the pole pieces of the electromagnet [3]

Fig. 3.3 Berkeley 184 in diameter, 4,000 ton cyclotron during construction [3]. The coil windings around both of the magnetic poles are clearly visible. Following the invention of longitudinal focusing it was actually operated as a synchrocyclotron, in 1946. The man on the right gives the scale
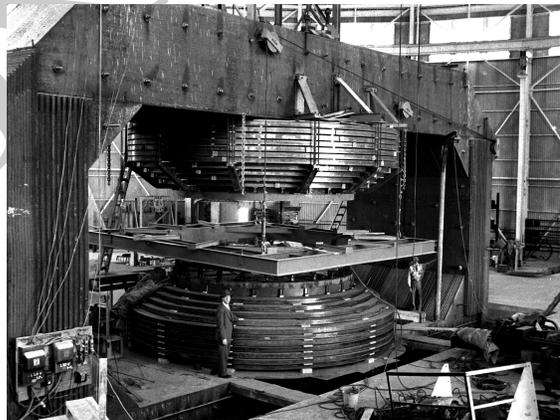
A broad range of applications were foreseen: *"At this time biological experiments were started. [...] Also at about this same time the first radioactive tracer experiments on human beings were tried [...] simple beginnings of therapeutic use, coming a little bit later, in which neutron radiation was used, for instance, in the treatment of cancer. [...] Another highlight from* 1936 *was the first time that anyone tried to make artificially a naturally occurring radio-nuclide.* (*a bismuth isotope*) [5, McMillan, p. 26].

Berkeley's 184 in cyclotron, the largest (Fig. 3.3), commissioned in 1941, was to accelerate Deuterons to 100 MeV for meson production. It's magnet however was diverted to the production of uranium for the atomic bomb during the second world war years [1]. Re-started in 1946, as a consequence of the discovery of phase focusing the accelerator was actually operated as a synchrocyclotron (an accelerator species addressed in Chap. 7).

Limitation in energy

The understanding of the dynamics of ions in the classical cyclotron took some time, and brought two news, a bad one and a good one,

(i) the bad one first: the energy limitation. A consequence of the loss of isochronism resulting from the relativistic increase of the ion mass so that *"[...] it seems useless to build cyclotrons of larger proportions than the existing ones [...] an accelerating chamber of* 37 *in radius will suffice to produce deuterons of* 11 *MeV energy which is the highest possible [...]"* [6], or in a different form: *"If you went to graduate school in the* 1940s*, this inequality* $(-1 < k < 0)$ *was the end of the discussion of accelerator theory"* [7].

(ii) the good news now: the energy limit which results from the mass increase can be removed by splitting the magnetic pole into valley and hill field sectors. This is the azimuthally varying field (AVF) cyclotron technology, due to L.H. Thomas in 1938 [8]. It took some years to see effects of this breakthrough (Fig. 3.4). The AVF is the object of Chap. 4.

With the progress in magnet computation tools, in computer speed and in beam dynamics simulations, the AVF cyclotron ends up being essentially as simple to design and build: it has in a general manner supplanted the classical cyclotron in all energy domains (Fig. 3.4).

3.2 Basic Concepts and Formulæ

The cyclotron was conceived as a means to overcome the technological difficulty of a long series of high electrostatic voltage electrodes in a linear layout, by, instead, repeated recirculation through a single accelerating gap in synchronism with an oscillating voltage (Fig. 3.5). As the accelerated bunch spirals out in the uniform magnetic field, the velocity increase comes with an increase in orbit length; the

number of
cyclotrons

a) classical cyclotrons
b) frequency modulated cyclotrons
c) AVF or sector focused cyclotrons
d) separated sector cyclotrons
e) superconducting cyclotrons
f) cyclotrons for commercial use

Fig. 3.4 Evolution of the number of the various cyclotron species, over the years [9]. From the 1950s on the AVF cyclotron rapidly supplanted the 1930s' classical cyclotron
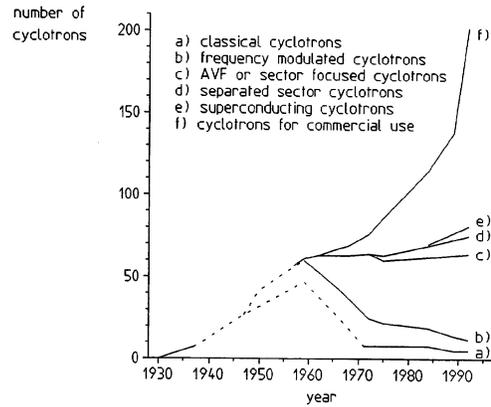
Fig. 3.5 Resonant acceleration: in an $h = 1$ configuration an ion bunch meets an oscillating field **E** across gap A, at time t, at an accelerating phase; it meets again, half a turn later, at time $t + T_{\rm rev}/2$, the accelerating phase across gap A', and so on: the magnetic field recirculates the bunch through the gap, repeatedly. Higher harmonic allows more bunches: the next possibility in the present configuration is h=3, and 3 bunches, 120 degrees apart, in synchronism with **E**
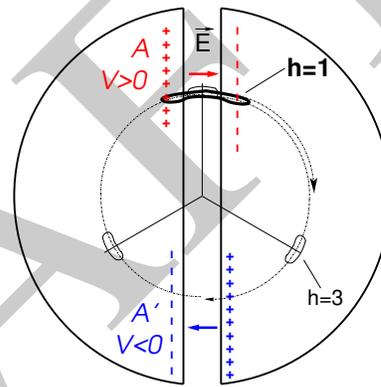
Fig. 3.6 An ion which reaches the double-dee gap at the RF phase $\omega_{\rm rf}t = \phi_A$ or $\omega_{\rm rf}t = \phi_B$ is accelerated. If it reaches the gap at $\omega_{\rm rf}t = \phi_C$ it is decelerated
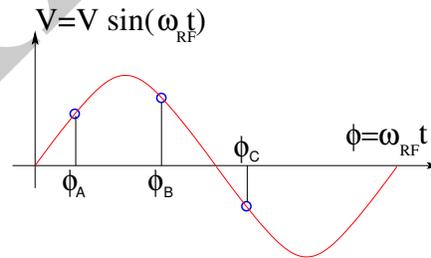
net result is a slow increase of the revolution period T_{rev} with energy, yet, with appropriate fixed $f_{\text{rf}} \approx h/T_{\text{rev}}$ the revolution motion and the oscillating voltage can be maintained in sufficiently close synchronism, $T_{\text{rev}} \approx T_{\text{rf}}/h$, that the bunch will transit the voltage gap at an accelerating phase (Fig. 3.6) over a large enough number of turns that it acquires a significant energy boost.

The orbital motion quantities: radius R, ion rigidity BR, revolution frequency f_{rev}, satisfy

$$BR = \frac{p}{q}, \qquad 2\pi f_{\text{rev}} = \omega_{\text{rev}} = \frac{v}{R} = \frac{qB}{m} = \frac{qB}{\gamma m_0} \tag{3.1}$$

These relationships hold at all γ, so covering the *classical* cyclotron domain ($v \ll c$, $\gamma \approx 1$) as well as the *isochronous* cyclotron (in which the ion energy increase is commensurate with its mass). To give an idea of the revolution frequency, in the limit $\gamma = 1$, for protons, one has $f_{\text{rev}}/B = q/2\pi m = 15.25\,\text{MHz/T}$.

The cyclotron design sets the constant RF frequency $f_{\text{rf}} = \omega_{\text{rf}}/2\pi$ at an intermediate value of $h f_{\text{rev}}$ along the acceleration cycle. The energy gain, or loss, by the ion when transiting the gap, at time t, is

$$\Delta W(t) = q\hat{V} \sin \phi(t) \quad \text{with} \quad \phi(t) = \omega_{\text{rf}} t - \omega_{\text{rev}} t + \phi_0 \tag{3.2}$$

with ϕ its phase with respect to the RF signal at the gap (Fig. 3.6), $\phi_0 = \phi(t = 0)$, and $\omega_{\text{rev}} t$ the orbital angle. Assuming constant field B, the increase of the revolution period with ion energy satisfies

$$\frac{\Delta T_{\text{rev}}}{T_{\text{rev}}} = \gamma - 1 \tag{3.3}$$

The mis-match so induced between the RF and cyclotron frequencies is a turn-by-turn cumulative effect and sets a limit to the tolerable isochronism defect, $\Delta T_{\text{rev}}/T_{\text{rev}} \approx 2 - 3\%$, or highest velocity $\beta = v/c \approx 0.22$. This results for instance in a practical limitation to $\approx 25\,\text{MeV}$ for protons, and $\approx 50\,\text{MeV}$ for D and α particles, a limit however dependent on energy gain per turn.

Over time multiple-gap accelerating structures where developed, whereby a "multiple-Δ" electrode pattern substitutes to a "double-D". An example is GANIL C0 injector with its 4 accelerating gaps and $h = 4$ and $h = 8$ RF harmonic operation [10].

3.2.1 Fixed-Energy Orbits, Revolution Period

In a laboratory frame (O;x,y,z), with (O;x,z) the bend plane (Fig. 3.7), assume $\mathbf{B}|_{y=0} = \mathbf{B}_y$, constant. An ion is launched from the origin with a velocity

$$\mathbf{v} = \left(\frac{dx}{dt}, \frac{dy}{dt}, \frac{dz}{dt} \right) = (v \sin \alpha, 0, v \cos \alpha)$$

at an angle α from the z-axis. Solving
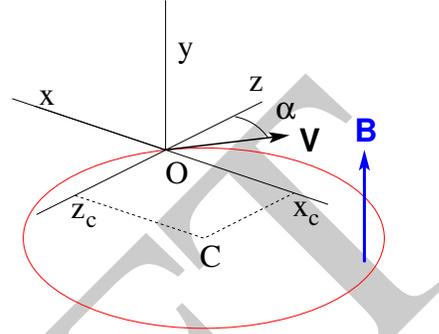
Fig. 3.7 Circular motion of an ion in the plane normal to a uniform magnetic field **B**. The orbit is centered at $x_C = -v \cos \alpha / \omega_{rev}$, $z_C = v \sin \alpha / \omega_{rev}$, its radius is v/ω_{rev}

$$m\dot{\mathbf{v}} = q\mathbf{v} \times \mathbf{B} \tag{3.4}$$

with $\mathbf{B} = (0, B_y, 0)$ yields the parametric equations of motion

$$
\begin{cases}
x(t) = \dfrac{v}{\omega_{rev}} \cos(\omega_{rev}t - \alpha) - \dfrac{v \cos \alpha}{\omega_{rev}} \\
y(t) = \text{constant} \\
z(t) = \dfrac{v}{\omega_{rev}} \sin(\omega_{rev}t - \alpha) + \dfrac{v \sin \alpha}{\omega_{rev}}
\end{cases}
\tag{3.5}
$$

which result in

$$\left(x + \frac{v \cos \alpha}{\omega_{rev}}\right)^2 + \left(z - \frac{v \sin \alpha}{\omega_{rev}}\right)^2 = \left(\frac{v}{\omega_{rev}}\right)^2 \tag{3.6}$$

a circular trajectory of radius $R = v/\omega_{rev}$ centered at $(x_C, z_C) = (-\frac{v \cos \alpha}{\omega_{rev}}, \frac{v \sin \alpha}{\omega_{rev}})$.

Stability of the cyclic motion - The initial velocity vector defines a reference closed orbit in the median plane of the cyclotron dipole; a small perturbation in α or v results in a new orbit *in the vicinity* of the reference. An axial velocity component v_y on the other hand, causes the ion to drift away from the reference, vertically, linearly with time, as is no axial restoring force. The next Section will investigate the necessary field property to ensure both horizontal and vertical confinement of the cyclic motion in the vicinity of a reference orbit in the median plane.

3.2.2 Weak Focusing

In the early accelerated turns in a classical cyclotron (central region of the electromagnet, energy up to tens of keV/u), the accelerating electric field provides vertical focusing for particles with proper RF phase [11, Sect. 8], whereas a flat magnetic field with uniformity $dB/B < 10^{-4}$ is sufficient to maintain isochronism. Beyond this low energy region however, at greater radii, a magnetic field gradient must be introduced to ensure transverse stability: field must decrease with R.

Fig. 3.8 Moving frame $(M_0; s, x, y)$ along the reference circular orbit. The curvature $1/R_0$ is constant along the orbit and $(M_0; s, x, y)$ can be considered equivalent to the cylindrical frame $(C; \theta, R_0, y)$
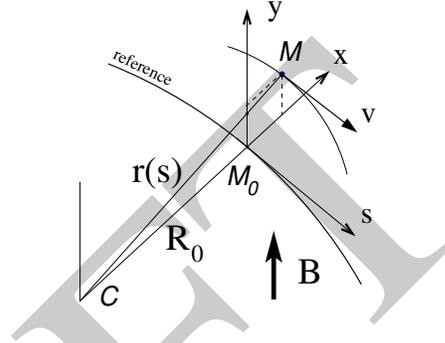
Ion coordinates in the following are defined in the moving frame $(M_0; s, x, y)$ (Fig. 3.8), which moves along the reference orbit (radius R_0), with its origin M_0 the projection of ion location M on the reference orbit; the s axis is tangent to the latter, the x axis is normal to s, the y axis is normal to the bend plane. Median-plane symmetry of the field is assumed, thus the radial field component $B_R|_{y=0} = 0$ at all R (Fig. 3.9).

Consider small motion excursions $x(t) = r(t) - R_0 \ll R_0$; introduce Taylor expansion of the field components,

$$B_y(R_0 + x) = B_y(R_0) + x \left.\frac{\partial B_y}{\partial R}\right|_{R_0} + \frac{x^2}{2!} \left.\frac{\partial^2 B_y}{\partial R^2}\right|_{R_0} + ... \approx B_y(R_0) + x \left.\frac{\partial B_y}{\partial R}\right|_{R_0}$$

$$B_R(0 + y) = y \underbrace{\left.\frac{\partial B_R}{\partial y}\right|_0}_{= \left.\frac{\partial B_y}{\partial R}\right|_{R_0}} + \frac{y^3}{3!} \left.\frac{\partial^3 B_R}{\partial y^3}\right|_0 + ... \approx y \left.\frac{\partial B_y}{\partial R}\right|_{R_0} \qquad (3.7)$$

Using these, and noting $(\dot{*}) = d(*)/dt$, the linear approximation of the differential equations of motion in the moving frame writes

$$F_x = m\ddot{x} = -qvB_y(R) + \frac{mv^2}{R_0 + x} \approx -qv\left(B_y(R_0) + \left.\frac{\partial B_y}{\partial R}\right|_{R_0} x\right) + \frac{mv^2}{R_0}\left(1 - \frac{x}{R_0}\right)$$

$$\rightarrow m\ddot{x} = -\frac{mv^2}{R_0^2}\left(\frac{R_0}{B_0}\left.\frac{\partial B_y}{\partial R}\right|_{R_0} + 1\right)x \tag{3.8}$$

$$F_y = m\ddot{y} = qvB_R(y) = qv\left.\frac{\partial B_R}{\partial y}\right|_{y=0} y + \text{higher order} \rightarrow m\ddot{y} = qv\frac{\partial B_y}{\partial R}y$$

Fig. 3.9 Axial motion stability requires proper shaping of field lines: B_y has to decrease with radius. The Laplace force pulls a positive charge with velocity pointing out of the page, at I, toward the median plane. Increasing the field gradient (k closer to -1, gap opening up faster) increases the focusing
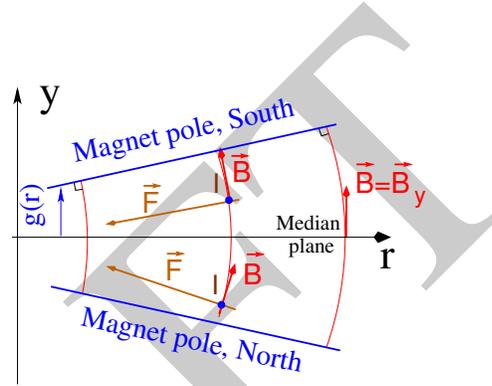
Fig. 3.10 Geometrical focusing: take k=0; two circular trajectories which start from $r = R_0 \pm \delta R$ (solid lines, going counter-clockwise) undergo exactly one oscillation around the reference orbit $r = R_0$. A negative k (triangles), for axial focusing, decreases the radial convergence; a positive k (square markers) increases the radial convergence - and increases vertical divergence
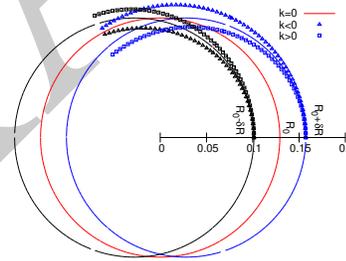
Note $B_y(R_0) = B_0$ and introduce

$$\omega_R^2 = \omega_{\text{rev}}^2\left(1 + \frac{R_0}{B_0}\frac{\partial B_y}{\partial R}\right), \quad \omega_y^2 = -\omega_{\text{rev}}^2 \frac{R_0}{B_0}\frac{\partial B_y}{\partial R} \tag{3.9}$$

substitute in Eqs. 3.8, this yields

Fig. 3.11 Radial motion stability. Trajectory arcs at $p = mv$ are represented: case of $k = 0$ (thin black lines), of $-1 < k < 0$ (thick blue lines), and of $k = -1$ (dashed concentric circles). k decreasing towards -1 reduces the geometrical focusing, increases axial focusing. The resultant of the Laplace and centrifugal forces, $F_t = -qvB + mv^2/r$, is zero at I, motion is stable if F_t is toward I at i, i.e. $qvB_i < mv^2/R_i$, and toward I as well at e, i.e. $qvB_e > mv^2/R_e$
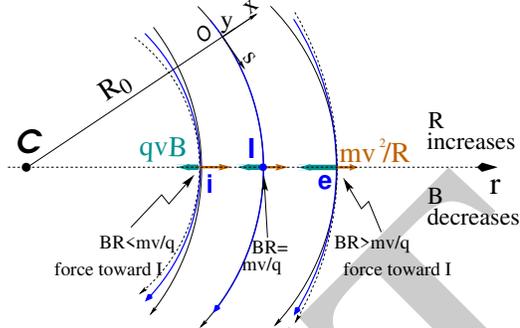
$$\ddot{x} + \omega_R^2 x = 0 \qquad \text{and} \qquad \ddot{y} + \omega_y^2 y = 0 \tag{3.10}$$

A restoring force (linear terms in x and y, Eq. 3.10) arises from the radially varying field, characterized by a field index

$$k = \frac{R_0}{B_0} \frac{\partial B_y}{\partial R}\bigg|_{R=R_0, y=0} \tag{3.11}$$

Radial stability: radially this force adds to the geometrical focusing (curvature term "1" in ω_R^2, Eq. 3.9, Fig. 3.10). In the weakly decreasing field $B(R)$ an ion with momentum $p = mv$ moving in the vicinity of the R_0-radius reference orbit experiences in the moving frame a resultant force $F_t = -qvB + m\frac{v^2}{r}$ (Fig. 3.11) of which the (outward) component $f_c = m\frac{v^2}{r}$ decreases with r at a higher rate than the decrease of the Laplace (inward) component $f_B = -qvB(r)$. In other words, radial stability requires BR to increase with R, $\frac{\partial BR}{\partial R} = B + R\frac{\partial B}{\partial R} > 0$, this holds in particular at R_0, thus $1 + k > 0$.

Axial stability requires a restoring force directed toward the median plane. Referring to Fig. 3.9, this means $F_y = -a \times y$ (with a a positive quantity) and thus $B_R < 0$, at all $(r, y \neq 0)$. This is achieved by designing a guiding field which decreases with radius, $\frac{\partial B_R}{\partial y} < 0$. Referring to Eq. 3.11 this means $k < 0$.

From these radial and axial constraints the condition of "weak focusing" for transverse motion stability around the circular equilibrium orbit results, namely,

$$-1 < k < 0 \tag{3.12}$$

Note regarding the geometrical focusing: the focal distance associated with the curvature of a magnet of arc length $\mathcal{L}$ is obtained by integrating $\frac{d^2x}{ds^2} + \frac{1}{R_0^2}x = 0$ and identifying with the focusing property $\Delta x' = -x/f$, namely,

$$\Delta x' = \int \frac{d^2x}{ds^2} ds \approx \frac{-x}{R^2} \int ds = \frac{-x\mathcal{L}}{R^2}, \text{ thus } f = \frac{R^2}{\mathcal{L}} \tag{3.13}$$

Isochronism: the axial focusing constraint, B decreasing with R, contributes breaking the isochronism (in addition to the effect of the mass increase) by virtue of $\omega_{\text{rev}} \propto B$.

Paraxial Transverse Coordinates

Introduce the path variable s as the independent variable in Eq. 3.10 and neglect the transverse velocity components ($1 + \frac{x}{R_0} \approx 1, \ y \ll 0$) so that

$$ds = \left[r^2(s)d\theta^2 + dr^2 + dy^2\right]^{1/2} \approx |\mathbf{v}|dt \tag{3.14}$$
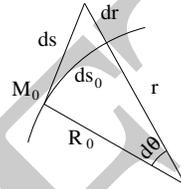
thus the equations of motion in the moving frame (Eq. 3.10) take the form

$$\frac{d^2x}{ds^2} + \frac{1+k}{R_0^2}x = 0 \quad \text{and} \quad \frac{d^2y}{ds^2} - \frac{k}{R_0^2}y = 0 \tag{3.15}$$

Given $-1 < k < 0$ the motion is that of a harmonic oscillator, in both planes, with respective restoring constants $(1+k)/R_0^2$ and $-k/R_0^2$, both positive quantities. The solution is a sinusoidal motion,

$$\begin{cases} r(s) - R_0 = x(s) = x_0 \cos \frac{\sqrt{1+k}}{R_0}(s-s_0) + x_0' \frac{R_0}{\sqrt{1+k}} \sin \frac{\sqrt{1+k}}{R_0}(s-s_0) \\ r'(s) = x'(s) = -x_0 \frac{\sqrt{1+k}}{R_0} \sin \frac{\sqrt{1+k}}{R_0}(s-s_0) + x_0' \cos \frac{\sqrt{1+k}}{R_0}(s-s_0) \end{cases} \tag{3.16}$$

$$\begin{cases} y(s) = y_0 \cos \frac{\sqrt{-k}}{R_0}(s-s_0) + y_0' \frac{R_0}{\sqrt{-k}} \sin \frac{\sqrt{-k}}{R_0}(s-s_0) \\ y'(s) = -y_0 \frac{\sqrt{-k}}{R_0} \sin \frac{\sqrt{-k}}{R_0}(s-s_0) + y_0' \cos \frac{\sqrt{-k}}{R_0}(s-s_0) \end{cases} \tag{3.17}$$

Radial and axial wave numbers can be introduced,

$$\nu_R = \frac{\omega_R}{\omega_{\text{rev}}} = \sqrt{1+k} \quad \text{and} \quad \nu_y = \frac{\omega_y}{\omega_{\text{rev}}} = \sqrt{-k} \tag{3.18}$$

i.e., the number of sinusoidal oscillations of the paraxial motion about the reference circular orbit over a turn, respectively radial and axial. Both are less than 1: there is less than one sinusoidal oscillation in a revolution. In addition, as a result of the revolution symmetry of the field,

$$\nu_R^2 + \nu_y^2 = 1 \tag{3.19}$$

Off-Momentum Orbit

In a structure with revolution symmetry, the equilibrium trajectory at momentum
$\begin{cases} p_0 \\ p = p_0 + \Delta p \end{cases}$ is at radius $\begin{cases} R_0 \text{ with } B_0 R_0 = \frac{p_0}{q} \\ R \text{ with } BR = \frac{p}{q} \end{cases}$, where $\begin{cases} B = B_0 + \left(\frac{\partial B}{\partial x}\right)_0 \Delta x + ... \\ R = R_0 + \Delta x \end{cases}$

On the other hand

$$BR = \frac{p}{q} \Rightarrow \left[B_0 + \left(\frac{\partial B}{\partial x}\right)_0 \Delta x + ... \right] (R_0 + \Delta x) = \frac{p_0 + \Delta p}{q}$$

which, neglecting terms in $(\Delta x)^2$, and given $B_0 R_0 = \frac{p_0}{q}$, leaves $\Delta x \left[\left(\frac{\partial B}{\partial x}\right)_0 R_0 + B_0 \right] = \frac{\Delta p}{q}$. With $k = \frac{R_0}{B_0} \left(\frac{\partial B}{\partial x}\right)_0$ this yields
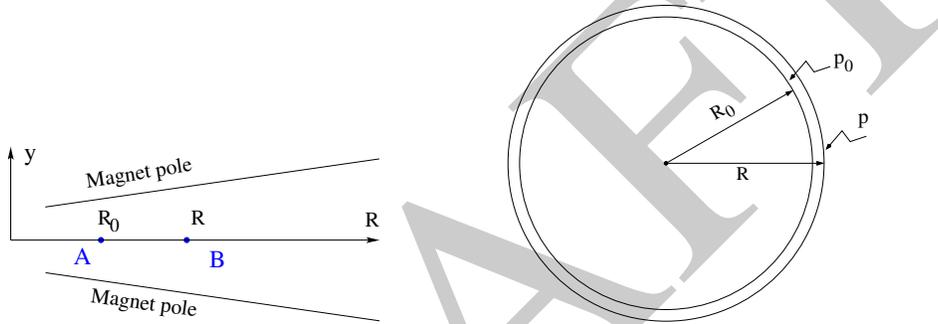
Fig. 3.12 The equilibrium radius at location A is R_0, momentum is p_0, rigidity is $B_0 R_0$. The equilibrium radius at B is R, momentum p, rigidity BR

$$\Delta x = D \frac{\Delta p}{p_0} \qquad \text{with} \qquad D = \frac{R_0}{1 + k} \qquad \text{the dispersion function} \qquad (3.20)$$

The dispersion D is an s-independent quantity as a result of the revolution symmetry
of the field (k and R=p/qB are s-independent).
To the first order in the coordinates, the vertical coordinates y(s), y'(s) (Eq. 3.17)
are unchanged under the effect of a momentum offset, the horizontal trajectory angle
x'(s) (Eq. 3.16) is unchanged as well (the circular orbits are concentric, Fig. 3.12)
whereas $x(s)$ satisfies

$$x(s, p_0 + \Delta p) = x(s, p_0) + \Delta p \left.\frac{\partial x}{\partial p}\right|_{s,p_0} = x(s, p_o) + D \frac{\Delta p}{p_0} \qquad (3.21)$$

Orbit and revolution period lengthening

1723 A δp momentum offset results in (Eq. 3.20)

$$\frac{\delta C}{C} = \frac{\delta R}{R} = \frac{\delta x}{R} = \alpha \frac{\delta p}{p} \quad \text{with} \quad \alpha = \frac{1}{1+k} = \frac{1}{\nu_R^2} \tag{3.22}$$

1724 with α the momentum compaction, a positive quantity: orbit length increases with
1725 momentum. Substituting $\frac{\delta \beta}{\beta} = \frac{1}{\gamma^2} \frac{\delta p}{p}$, the change in revolution period $T_{\text{rev}} = C/\beta c$
1726 with momentum writes

$$\frac{\delta T_{\text{rev}}}{T_{\text{rev}}} = \frac{\delta C}{C} - \frac{\delta \beta}{\beta} = \left(\alpha - \frac{1}{\gamma^2} \right) \frac{\delta p}{p} \tag{3.23}$$

1727 Given that $-1 < k < 0$ and $\gamma \gtrsim 1$, it results that $\alpha - 1/\gamma^2 > 0$: the revolution period
1728 increases with energy, the increase in radius is faster than the velocity increase.

3.2.3 Quasi-Isochronous Resonant Acceleration

1730 The energy W of an accelerated ion (in the non-relativistic energy domain of the
1731 classical cyclotron) satisfies the frequency dependence

$$W = \frac{1}{2}mv^2 = \frac{1}{2}m\left(2\pi R f_{\text{rev}}\right)^2 = \frac{1}{2}m\left(2\pi R \frac{f_{\text{rf}}}{h}\right)^2 \tag{3.24}$$

1732 Observe in passing: given the cyclotron size (radius R), f_{rf} and h set the limit for
1733 the acceleration range. The revolution frequency decreases with energy and the
1734 condition of synchronism with the oscillating voltage, $f_{\text{rf}} = h f_{\text{rev}}$, is only fulfilled
1735 at that particular radius where $\omega_{\text{rf}} = qB/m$ (Fig. 3.13-left). The out-phasing $\Delta\phi$ of
1736 the RF at ion arrival at the gap builds-up turn after turn, decreasing in a first stage
1737 (towards lower voltages in Fig. 3.13-right) and then increasing back to $\phi = \pi/2$ and
1738 beyond towards π. Beyond $\phi = \pi$ the RF voltage is decelerating.
1739   With ω_{rev} constant between two gap passages, differentiating $\phi(t)$ (Eq. 3.2) yields
1740 $\dot\phi = \omega_{\text{rf}} - \omega_{\text{rev}}$. Between two gap passages on the other hand, $\Delta\phi = \dot\phi \Delta T = \dot\phi T_{\text{rev}}/2 =$
1741 $\dot\phi \frac{\pi R}{v}$, yielding a phase-shift of

$$\text{half-turn} \quad \Delta\phi = \pi \left(\frac{\omega_{\text{rf}}}{\omega_{\text{rev}}(R)} - 1 \right) = \pi \left(\frac{m\omega_{\text{rf}}}{qB(R)} - 1 \right) \tag{3.25}$$

1742 The out-phasing is thus a gap-after-gap, cumulative effect. Due to this the classical
1743 cyclotron requires quick acceleration (small number of turns), which means high
1744 voltage (tens to hundreds of kVolts). As expected, with ω_{rf} and B constant, ϕ presents
1745 a minimum ($\dot\phi = 0$) at $\omega_{\text{rf}} = \omega_{\text{rev}} = qB/m$ where exact isochronism is reached
1746 (Fig. 3.13). The upper limit to ϕ is set by the condition $\Delta W > 0$: acceleration.
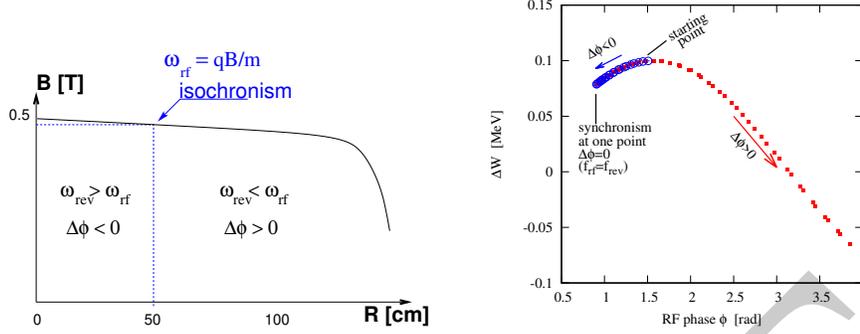
Fig. 3.13 Left: a sketch of the synchronism condition at one point (h=1 assumed). Right: the span in phase of the energy gain $\Delta W = q\hat{V}\sin\phi$ (Eq. 3.2) over the acceleration cycle

Fig. 3.14 A graph of the cyclotron equation (Eq. 3.26), for three different accelerating voltages: 100, 200 and 400 kV/gap (respectively square, circle and triangle markers). The sole settings resulting in $-1 < \cos\phi(E) < 1$, $\forall E$, allow complete acceleration to top energy. $\phi_i = \pi/4$ at injection for instance, does not (upper three curves). $\phi_i = 3\pi/4$ works (lower three curves), with as low as 100 kV/gap
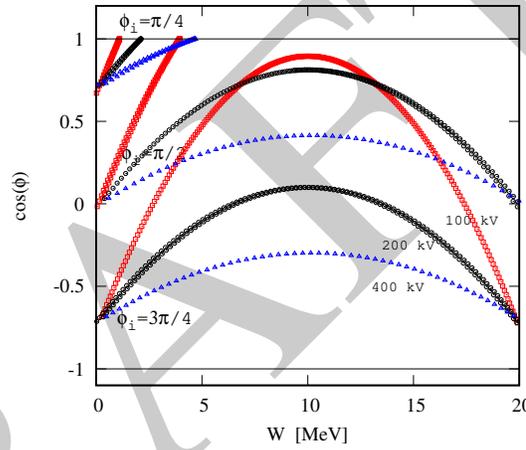
The cyclotron equation determines the achievable energy range, depending on the injection energy E_i, the RF phase at injection ϕ_i, the RF frequency $\omega_{\rm rf}$ and gap voltage $\hat{V}$. It writes [12]

$$\cos\phi = \cos\phi_i + \pi\left[1 - \frac{\omega_{\rm rf}}{\omega_{\rm rev}}\frac{E+E_i}{2M}\right]\frac{E-E_i}{q\hat{V}} \tag{3.26}$$

Equation 3.26 is represented in Fig. 3.14 for various values of the peak voltage and phase at injection ϕ_i. M [eV/c^2] and E [eV] are respectively the rest mass and relativistic energy, $q\hat{V}$ is expressed in electron-volts, the index i denotes injection parameters.

1754 ### 3.2.4 Beam Extraction

1755 From $R = p/qB$ and assuming $B(R) \approx$ constant (this is legitimate as k is normally
1756 small), in the non-relativistic approximation ($W \ll M$, $W = p^2/2M$) one gets

$$\frac{dR}{R} = \frac{1}{2}\frac{dW}{W} \tag{3.27}$$

1757 Integrating yields

$$R^2 = R_i^2 \frac{W}{W_i} \tag{3.28}$$

1758 with R_i, W_i initial conditions. From Eqs. 3.27, 3.28, assuming $W_i \ll W$ and constant
1759 acceleration rate dW such that $W = n\, dW$ after n turns, one gets the scaling laws

$$R \propto \sqrt{n}, \qquad dR \propto \frac{R}{W} \propto \frac{1}{R} \propto dW, \qquad \frac{dR}{dn} = \frac{R}{2n} \tag{3.29}$$

1760 The turn separation dR is proportional to the energy gain per turn and inversely
1761 proportional to the orbit radius.
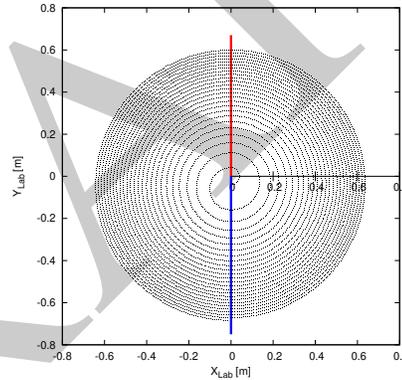
Fig. 3.15 The radial distance between successive turns decreases with energy, in inverse proportion to the orbit radius. The red and blue segments here figure the accelerating gap

1762   The radial distance between successive turns decreases with energy, toward zero
1763 (Fig. 3.15), eventually resulting in insufficient spacing for insertion of an extraction
1764 septum.

1765 *Orbit modulation*

1766 Consider an ion bunch injected in the cyclotron with some (x_0, x_0') conditions in
1767 the vicinity of the reference orbit, and assume slow acceleration. While accelerated
1768 the bunch undergoes an oscillatory motion around the equilibrium orbit (Eq. 3.16).
1769 Observed at the extraction septum this oscillation modulates the distance of the

bunch to the local equilibrium orbit, moving it outwards or inwards depending on the turn number, which modulates the distance between the accelerated turns. This effect can be resorted to, so to increase the separation between the final two turns and so enhance the extraction efficiency [9].

3.2.5 Spin Dance

"Much of the physics of spin motion can be illustrated using the simplest model of a storage ring consisting of uniform horizontal bending and no straight sections." [13].

By virtue of this statement, a preliminary introduction to spin motion in magnetic fields is given in the present chapter. In support to this in addition, comes the fact that cyclotrons happened to be the first circular machines to acelerate polarized beams (first acceleration of polarized beams had happened earlier in the 1960s, using electrostatic columns at voltage generators, when polarized proton and deuteron sources began operating [14]).

The magnetic field $\mathbf{B}$ of the cyclotron dipole exerts a torque on the spin angular momentum $\mathbf{S}$ of an ion, causing it to precess following the Thomas-BMT differential equation [15]

$$\frac{d\mathbf{S}}{dt} = \mathbf{S} \times \underbrace{\frac{q}{m} \left[(1 + G)\mathbf{B}_{\parallel} + (1 + G\gamma)\mathbf{B}_{\perp} \right]}_{\boldsymbol{\omega}_{\text{sp}}} \tag{3.30}$$

where t is the time; $\boldsymbol{\omega}_{\text{sp}}$ the precession vector: a combination of $\mathbf{B}_{\parallel}$ and $\mathbf{B}_{\perp}$ components of $\mathbf{B}$ respectively parallel and orthogonal to the ion velocity vector. G is the gyromagnetic anomaly,

G=1.7928474 (proton), -0.178 (Li), -0.143 (deuteron), -4.184 (^{3}He) ...

$\mathbf{S}$ in this equation is in the ion rest frame, all other quantities are in the laboratory frame.

In the case of an ion moving in the median plane of the dipole, $\mathbf{B}_{\parallel} = 0$, thus the precession axis is parallel to the magnetic field vector, $\mathbf{B}_y$, so that $\omega_{\text{sp}} = \frac{q}{m}(1 + G\gamma)\mathbf{B}_y$. The spin precession angle over a trajectory arc $\mathcal{L}$ is

$$\theta_{\text{sp, Lab}} = \frac{1}{v} \int_{(\mathcal{L})} \omega_{\text{sp}} \, ds = (1 + G\gamma) \frac{\int_{(\mathcal{L})} B \, ds}{BR} = (1 + G\gamma)\alpha \tag{3.31}$$

with α the velocity vector precession (Fig. 3.16). The precession angle in the moving frame (the latter rotates by an angle α along $\mathcal{L}$) is

$$\theta_{\text{sp}} = G\gamma\alpha \tag{3.32}$$

thus the number of 2π spin precessions per ion orbit around the cyclotron is $G\gamma$. By analogy with the wave numbers (Eq. 3.18) this defines the "spin tune"

Fig. 3.16 Spin and velocity vector precession in a constant field, from **S** to **S'** and **v** to **v'** respectively. In the moving frame the spin precession along the arc $\mathcal{L} = R\alpha$ is $G\gamma\alpha$, in the laboratory frame the spin precesses by $(1 + G\gamma)\alpha$
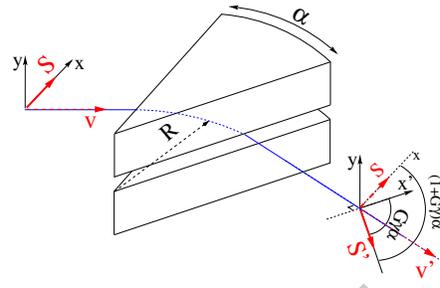
$$\nu_{\text{sp}} = G\gamma \qquad\qquad (3.33)$$

3.3 Exercises

Note: some of the input data files for these simulations are available in zgoubi sourceforge repository at
https://sourceforge.net/p/zgoubi/code/HEAD/tree/branches/exemples/book/zgoubiMaterial/cyclotron_classical/

3.1 Modeling a Cyclotron Dipole: Using a Field Map

Solution: page 71

In this exercise, ion trajectories are ray-traced, various optical properties addressed in the foregoing are recovered, using a field map to simulate the cyclotron dipole. Fabricating that field map is a preliminary step of the exercise.

The interest of using a field map is that it is an easy way to account for fancy magnet geometries and fields, including field gradients and possible defects. A field map can be generated using mathematical field models, or from magnet computation codes, or from magnetic measurements. The first method is used, here. TOSCA[MOD.MOD1=22.1] keyword [16, *cf.* INDEX] is used to ray-trace through the map.

Working hypotheses: A 2-dimensional $m(R, \theta)$ polar meshing of the median plane is considered (Fig. 3.17). It is defined in a $(O; X, Y)$ frame and covers an angular sector of a few tens of degrees. The mid-plane field map is the set of values $B_Z(R, \theta)$ at the nodes of the mesh. During ray-tracing, TOSCA[MOD.MOD1=22.1] extrapolates the field along 3D space (R, θ, Z) ion trajectories from the 2D polar map [16].

Fig. 3.17 Principle of a 2D field map in polar coordinates, covering a 180° sector (over the right hand side dee). The mesh nodes $m(R, \theta)$ are distant ΔR radially, $\Delta\theta$ azimuthally. The map is used twice to cover the 360° cyclotron dipole as sketched here, while allowing insertion of an accelerating gap between the two dees
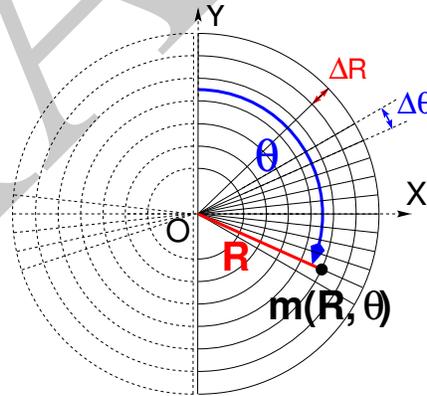
(a) Construct a 180° two-dimensional map of a median plane field $B_Z(R, \theta)$, proper to simulate the field in a cyclotron as sketched in Fig. 3.1. Use one of the following two methods: either (i) write an independent program, or (ii) use zgoubi and its analytical field model DIPOLE, together with the keyword OPTIONS[CONSTY=ON] [16, *cf.* INDEX].

Besides: use a uniform mesh (Fig. 3.17) covering from Rmin=1 to Rmax=76 cm, with radial increment $\Delta R = 0.5$ cm, azimuthal increment $\Delta\theta = 0.5$ [cm]/R_0 with R_0

some reference radius (say, 50 cm, in view of subsequent exercises), and constant axial field $B_Z = 5$ kG. The appropriate 6-column formatting of the field map data for TOSCA[MOD.MOD1=22.1] to read is the following:

$$R \cos \theta, \ Z, \ R \sin \theta, \ BY, \ BZ, \ BX$$

with θ varying first, R varying second; Z is the vertical direction (normal to the map mesh), $Z \equiv 0$ in the present case. Note that proper functioning of TOSCA requires the field map to begin with the following line of numerical values:

$$\text{Rmin [cm]} \quad \Delta R \text{ [cm]} \quad \Delta \theta \text{ [deg]} \quad Z \text{ [cm]}$$

Produce a graph of the $B_Z(R, \theta)$ field map content.

(b) Ray-trace a few concentric circular mid-plane trajectories centered on the center of the dipole, ranging in $10 \le R \le 80$ cm. Produce a graph of these concentric trajectories in the $(O; X, Y)$ laboratory frame.

Initial coordinates can be defined using OBJET, particle coordinates along trajectories during the stepwise ray-tracing can be logged in zgoubi.plt by setting IL=2 under TOSCA. In order to find the Larmor radius corresponding to a particular momentum, the matching procedure FIT can be used. In order to repeat the latter for a series of different momenta, REBELOTE[IOPT=1] can be used.

Explain why it is possible to push the ray-tracing beyond the 76 cm radial extent of the field map.

(c) Compute the orbit radius R and the revolution period T_{rev} as a function of kinetic energy W or rigidity BR. Produce a graph, including for comparison the theoretical dependence of T_{rev}.

(d) Check the effect of the density of the mesh (the choice of ΔR and $\Delta \theta$ values, *i.e.*, the number of nodes $N_\theta \times N_R = (1 + \frac{180^o}{\Delta \theta}) \times (1 + \frac{80 \text{ cm}}{\Delta R})$), on the accuracy of the trajectory and time-of-flight computation.

(e) Check the effect of the integration step size on the accuracy of the trajectory and time-of-flight computation, by considering a small $\Delta s = 1$ cm and a large $\Delta s = 10$ cm, at 200 keV and 5 MeV (proton), and comparing with theory.

(f) Consider a periodic orbit, thus its radius R should remain unchanged after stepwise integration of the motion over a turn. However, the size Δs of the numerical integration step has an effect on the final value of the radius:

For two different cases, 200 keV (a small orbit) and 5 MeV (a larger one), provide a graph of the dependence of the relative error $\delta R/R$ after one turn, on the integration step size Δs (consider a series of Δs values in a range $\Delta s : 0.1$ mm $\rightarrow 20$ cm). REBELOTE[IOPT=1] do-loop can be used to repeat the one-turn raytracing with different Δs.

3.2 Modeling a Cyclotron Dipole: Using an Analytical Field Model

Solution: page 80

This exercise is similar to exercise 3.1, yet using the analytical modeling DIPOLE, instead of a field map. DIPOLE provides the Z-parallel median plane field $\mathbf{B}(R, \theta, Z = 0) \equiv \mathbf{B}_Z(R, \theta, Z = 0)$ at the projected $m(R, \theta, Z = 0)$ ion location (Fig. 3.18), while $\mathbf{B}(R, \theta, Z)$ at particle location is obtained by extrapolation.
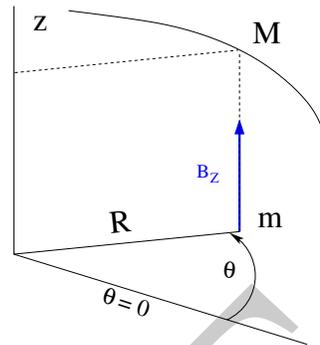
Fig. 3.18 DIPOLE provides the value $B_Z(m)$ of the median plane field at m, projection of particle position $M(R, \theta, Z)$ in the median plane. $\mathbf{B}(R, \theta, Z)$ is obtained by extrapolation

(a) Simulate a 180° sector dipole; DIPOLE requires a reference radius [16, Eqs. 6.3.19-21], noted R_0 here; for the sake of consistency with other exercises, it is suggested to take $R_0 = 50$ cm. Take a constant axial field $B_Z = 5$ kG.

Explain the various data that define the field simulation in DIPOLE: geometry, role of R_0, field and field indices, fringe fields, integration step size, etc.

Produce a graph of $B_Z(R, \theta)$.

(b) Repeat question (b) of exercise 3.1.

(c) Repeat question (c) of exercise 3.1.

(d) As in question (e) of exercise 3.1, check the effect of the integration step size on the accuracy of the trajectory and time-of-flight computation.

Repeat question (f) of exercise 3.1.

(e) From the two series of results (exercise 3.1 and the present one), comment on various pros and cons of the two methods, field map versus analytical field model.

3.3 Resonant Acceleration

Solution: page 84

Based on the earlier exercises, using indifferently a field map (TOSCA) or an analytical model of the field (DIPOLE), introduce a sinusoidal voltage between the two dees, with peak value 100 kV. Assume that ion motion does not depend on RF phase: the boost through the gap is the same at all passes, use CAVITE[IOPT=3] [16, *cf.* INDEX] for that. Note that using CAVITE requires prior PARTICUL in order to specify ion species and data, necessary to compute the energy boost (Eq. 3.2).

(a) Accelerate a proton with initial kinetic energy 20 keV, up to 5 MeV, take harmonic h=1. Produce a graph of the accelerated trajectory in the laboratory frame.

(b) Provide a graph of the proton momentum p and total energy E as a function of its kinetic energy, both from this numerical experiment (ray-tracing data can be stored using FAISTORE) and from theory, all on the same graph.

(c) Provide a graph of the normalized velocity $\beta = v/c$ as a function of kinetic energy, both numerical and theoretical, and in the latter case both classical and relativistic.

1897 (d) Provide a graph of the relative change in velocity $\Delta\beta/\beta$ and orbit length $\Delta C/C$
1898 as a function of kinetic energy, both numerical and theoretical. From their evolution,
1899 conclude that the time of flight increases with energy.

1900 (e) Repeat the previous questions, assuming a harmonic h=3 RF frequency.

3.4 Spin Dance
1902 Solution: page 88

1903 Cyclotron modeling in the present exercise can use Exercise 3.1 or Exercise 3.2
1904 technique (*i.e.*, a field map or an analytical field model), indifferently.

1905 (a) Add spin transport, using SPNTRK [16, *cf.* INDEX]. Produce a listing
1906 (zgoubi.res) of a simulation, including spin outcomes.

1907 Note: PARTICUL is necessary here, for the spin equation of motion (Eq. 3.30) to
1908 be solved [16, Sect. 2]. SPNPRT can be used to have local spin coordinates listed in
1909 zgoubi.res (at the manner that FAISCEAU lists local particle coordinates).

1910 (b) Consider proton case, take initial spin longitudinal, compute the spin preces-
1911 sion over one revolution, as a function of energy over a range 12 keV→5 MeV. Give
1912 a graphical comparison with theory.

1913 FAISTORE can be used to store local particle data, which include spin coor-
1914 dinates, in a zgoubi.fai style output file. IL=2 [16, *cf.* INDEX] (under DIPOLE or
1915 TOSCA, whichever modeling is used) can be used to obtain a print out of particle
1916 and spin motion data to zgoubi.plt during stepwise integration.

1917 (c) Inject a proton with longitudinal initial spin $\mathbf{S}_i$. Give a graphic of the lon-
1918 gitudinal spin component value as a function of azimuthal angle, over a few turns
1919 around the ring. Deduce the spin tune from this computation. Repeat for a couple of
1920 different energies.

1921 Place both FAISCEAU and SPNPRT commands right after the first dipole sector,
1922 and use them to check the spin rotation and its relationship to particle rotation, right
1923 after the first passage through that first sector.

1924 (d) Spin dance: the input data file optical sequence here is assumed to model a
1925 full turn. Inject an initial spin at an angle from the horizontal plane (this is in order
1926 to have a non-zero vertical component), produce a 3-D animation of the spin dance
1927 around the ring, over a few turns.

1928 (e) Repeat questions (b-d) for two additional ions: deuteron (much slower spin
1929 precession), $^3He^{2+}$ (much faster spin precession).

3.5 Synchronized Spin Torque
1931 Solution: page 94

1932 A synchronized spin kick is superimposed on orbital motion. An input data file for
1933 a complete cyclotron is considered as in question 3.4 (d), for instance six 60 degree
1934 DIPOLEs, or two 180 degree DIPOLEs.

1935 Insert a local spin rotation of a few degrees around the longitudinal axis, at the
1936 end of the optical sequence (*i.e.*, after one orbit around the cyclotron). SPINR can be
1937 used for that, rather than a local magnetic field, so to avoid any orbital effect. Track
1938 4 particles on their respective equilibrium orbit, with energies 0.2, 108.412, 118.878
1939 and 160.746 MeV.

Produce a graph of the motion of the vertical spin component S_y along the circular orbit.

Produce a graph of the spin vector motion on a sphere.

3.6 Weak Focusing

Solution: page 97

(a) Consider a 60° sector as in earlier exercises (building a field map and using TOSCA as in exercise 3.1, or using DIPOLE as in exercise 3.2), construct the sector accounting for a non-zero radial index k in order to introduce axial focusing, say $k = -0.03$, assume a reference radius R_0 for a reference energy of 200 keV (R_0 and B_0 are required in order to define the index k, Eq. 3.11). Ray-trace that 200 keV reference orbit, plot it in the lab frame: make sure it comes out as expected, namely, constant radius, final and initial angles zero.

(b) Using FIT[2], find and plot the radius dependence of orbit rigidity, $BR(R)$, from ray-tracing over a BR range covering 20 keV to 5 MeV; superpose the theoretical curve. REBELOTE[IOPT=1] can be used to perform the scan.

(c) Produce a graph of the paraxial axial motion of a 1 MeV proton, over a few turns (use IL=2 under TOSCA, or DIPOLE, to have step by step particle and field data logged in zgoubi.plt). Check the effect of the focusing strength by comparing the trajectories for a few different index values, including close to -1 and close to 0.

(d) Produce a graph of the magnetic field experienced by the ion along these trajectories.

3.7 Loss of Isochronism

Solution: page 106

Compare on a common graphic the revolution period $T_{\rm rev}(R)$ for a field index value $k \approx -0.95,\ -0.5,\ -0.03,\ 0^-$. The scan method of exercise 3.6, based on REBELOTE[IOPT=1] preceded by FIT[2], can be referred to.

3.8 Ion Trajectories

Solution: page 108

In this exercise individual ion trajectories are computed. DIPOLE or TOSCA magnetic field modeling can be used, indifferently. No acceleration here, ions circle around the cyclotron at constant energy.

(a) Produce a graph of the horizontal $x(s)$ and vertical $y(s)$ trajectory coordinates of an ion with rigidity $BR(R_0)$ (R_0 is the 200 keV reference radius in the definition of the index k), over a few turns around the cyclotron. From the number of turns, give an estimate of the wave numbers. Check the agreement with the expected $\nu_R(k)$, $\nu_y(k)$ values (Eq. 3.18).

(b) Consider now protons at 1 MeV and 5 MeV, far from the reference energy $E(R_0)$; the wave numbers change with energy: consistency with theory can be checked. Find their theoretical values, compare with numerical outcomes.

(c) Consider proton, 200 keV energy, plot as a function of s the difference between $x(s)$ from raytracing and its values from Eq. 3.16. Same for y(s) compared to Eq. 3.17.

1981 IL=2 can be used to store in zgoubi.plt the step-by-step particle coordinates across
1982 DIPOLE.

1983   (d) Perform a scan of the wave numbers over $200\,\mathrm{keV} - 5\,\mathrm{MeV}$ energy inter-
1984 val, computed using OBJET[KOBJ=5] and MATRIX[IORD=1,IFOC=11], or OB-
1985 JET[KOBJ=6] and MATRIX[IORD=2,IFOC=11], together with REBELOTE[IOPT=1]
1986 to repeat MATRIX for a series of energy values.

1987 3.9 RF Phase at the Accelerating Gap

1988   Solution: page 114

1989   Consider the cyclotron model of exercise 3.6: field index $k = -0.03$ defined at
1990 $R_0 = 50\,\mathrm{cm}$, field $B_0 = 5\,kG$ on that radius. two dees, double accelerating gap.

1991   Accelerate a proton from 1 to 5 MeV: get the turn-by-turn phase-shift at the gaps;
1992 use CAVITE[IOPT=7] to simulate the acceleration. Compare the half-turn $\Delta\phi$ so
1993 obtained with the theoretical expectation (Eq. 3.25). Produce similar graphs $B(R)$
1994 and $\Delta W(\phi)$ to Fig. 3.13.

1995   Accelerate over more turns, observe the particle decelerating.

1996 3.10 The Cyclotron Equation

1997   Solution: page 116

1998   The cyclotron model of exercise 3.3 is considered: two dees, double accelerating
1999 gap, uniform field $B = 5\,\mathrm{kG}$, no field gradient needed here (no vertical motion).

2000   (a) Set up an input data file for the simulation of a proton acceleration from
2001 0.2 to 20 MeV. In particular, assume that $\cos(\phi)$ reaches its maximum value at
2002 $W_m = 10\,\mathrm{MeV}$; find the RF voltage frequency from $d(\cos\phi)/dW = 0$ at W_m.

2003   (b) Give a graph of the energy-phase relationship (Eq. 3.26), for $\phi_i = \frac{3\pi}{4}, \frac{\pi}{2}, \frac{\pi}{4}$,
2004 from both simulation and theory.

2005 3.11 Cyclotron Extraction

2006   Solution: page 118

2007   (a) Acceleration of a proton in a uniform field $B = 5\,\mathrm{kG}$ is first considered (field
2008 hypotheses as in exercise 3.3). RF phase is ignored: CAVITE[IOPT=3] can be used
2009 for acceleration. Take a 100 kV gap voltage.

2010   Compute the distance ΔR between turns, as a function of turn number and of
2011 energy, over the range $E : 0.02 \rightarrow 5\,\mathrm{MeV}$. Compare graphically with theoretical
2012 expectation.

2013   (b) Assume a beam with Gaussian momentum distribution and *rms* momentum
2014 spread $\delta p/p = 10^{-3}$. An extraction septum is placed half-way between two successive
2015 turns, provide a graph of the percentage of beam loss at extraction, as a function of
2016 extraction turn number. COLLIMA can be used for that simulation and for particle
2017 counts, it also allows for possible septum thickness.

2018   (c) Repeat (a) and (b) considering a field with index: take for instance $B_0 = 5\,\mathrm{kG}$
2019 and $k = -0.03$ at $R_0 = R(0.2\,\mathrm{MeV}) = 12.924888\,\mathrm{cm}$.

2020   (d) Investigate the effect of injection conditions (Y_i, T_i) on the modulation of the
2021 distance between turns.

²⁰²² Try and confirm numerically that, with slow acceleration, the oscillation is mini-
²⁰²³ mized for an initial $|T_i| = |\frac{x_0 \nu_R}{R}|$ (after Ref. [9, p. 133]).

²⁰²⁴ 3.12 Acceleration and Extraction of a 6-D Polarized Bunch

²⁰²⁵ Solution: page 123

²⁰²⁶ The cyclotron simulation hypotheses of exercise 3.10-a are considered; account
²⁰²⁷ or $k = -0.02$ field index.

²⁰²⁸ Add a short "high energy" extraction line, say 1 meter, following REBELOTE in
²⁰²⁹ the optical sequence, ending up with a "Beam_Dump" MARKER for instance.

²⁰³⁰ (a) Create a 1,000 ion bunch with the following initial parameters:

²⁰³¹ - random Gaussian transverse phase space densities, centered on the equilibrium
²⁰³² orbit, truncated at 3 sigma, normalized *rms* emittances $\varepsilon_Y = \varepsilon_Z = 1 \pi \mu$m, both
²⁰³³ emittances matched to the 0.2 MeV orbit optics,

²⁰³⁴ - uniform bunch momentum density $0.2 \times (1 - 10^{-3}) \leq p \leq 0.2 \times (1 + 10^{-3})$ MeV,
²⁰³⁵ matched to the dispersion, namely (Eq. 3.21), $\Delta x = D\frac{\Delta p}{p}$,

²⁰³⁶ - random uniform longitudinal distribution $-0.5 \leq s \leq 0.5$ mm,

²⁰³⁷ Note: two ways to create this object are, (i) using MCOBJET[KOBJ=3] which
²⁰³⁸ generates a random distribution, or (ii) using OBJET[KOBJ=3] to read an external
²⁰³⁹ particle coordinate file.

²⁰⁴⁰ Add spin tracking request (SPNTRK), all initial spins normal to the bend plane.

²⁰⁴¹ Produce a graph of the three initial 2-D phase spaces: (Y,T), (Z,P), ($\delta l,\delta p/p$),
²⁰⁴² matched to the 200 keV periodic optics. Provide Y, Z, dp/p, δl and S_Z histograms
²⁰⁴³ (HISTO can be used), check the distribution parameters.

²⁰⁴⁴ (b) Accelerate this polarized bunch to 20 MeV, using the following RF conditions:

²⁰⁴⁵ - 200 kV peak voltage,

²⁰⁴⁶ - RF harmonic 1,

²⁰⁴⁷ - initial RF phase $\phi_i = \pi/4$.

²⁰⁴⁸ Produce a graph of the three phase spaces as observed downstream of the extrac-
²⁰⁴⁹ tion line. Provide the Y, Z, dp/p, δl and S_Z histograms. Compare the distribution
²⁰⁵⁰ parameters with the initial values.

²⁰⁵¹ What causes the spins to spread away from vertical?

²⁰⁵² 3.4 Solutions of Exercises of Chapter 3: Classical Cyclotron

²⁰⁵³ 3.1 Modeling a Cyclotron Dipole: Using a Field Map

²⁰⁵⁴

²⁰⁵⁵ (a) A field map of a 180° sector of a classical cyclotron magnet.

²⁰⁵⁶ The first option is retained here: a Fortran program, geneSectorMap.f, given in
²⁰⁵⁷ Tab. 3.1. constructs the required map of a field distribution $B_Z(R, \theta)$, to be subse-
²⁰⁵⁸ quently read and raytraced through using the keyword TOSCA [16, *lookup* INDEX].